Remote Sensing of Environment 183 (2016) 282–293

Contents lists available at ScienceDirect

Remote Sensing of Environment

journal homepage: www.elsevier.com/locate/rse

The impact of satellite sensor viewing geometry on time-series analysis of volcanic emissions

Verity J.B. Flower [a,*], Simon A. Carn [a], Robert Wright [b]

[a] Dept. of Geological and Mining Engineering and Sciences, Michigan Technological University, 1400 Townsend Dr, Houghton, MI 49931, USA
[b] Hawaii Institute of Geophysics and Planetology, University of Hawaii at Manoa, Honolulu, HI 96822, USA

ARTICLE INFO

Article history:
Received 20 November 2015
Received in revised form 9 May 2016
Accepted 28 May 2016
Available online 13 June 2016

Keywords:
Time-series analysis
Satellite remote sensing
Volcanic emissions
OMI
MODIS

ABSTRACT

Time-series analysis techniques are being increasingly used to process satellite observations of volcanic gas emissions and heat flux, with the aim of identifying cyclic behaviour that could inform hazard assessment or elucidate volcanic processes. However, it can be difficult to distinguish cyclic variations due to geophysical processes from those that are artefacts of the observation technique. Here, we conduct a comprehensive investigation into the origin of cyclicity in volcanic observations by analysing daily, global satellite measurements of volcanic SO_2 loading by the Ozone Monitoring Instrument (OMI) and thermal infrared anomalies detected by the Moderate Resolution Imaging Spectroradiometer (MODIS). We use a fast Fourier Transform (FFT) multi-taper method (MTM) to analyse multiple phases of activity at 32 target volcanoes, utilising measurements obtained from three NASA satellite instruments (Aura – OMI, Aqua – MODIS and Terra – MODIS), and identify a common cycle (period of ~2.3 days), which is not considered to be of volcanic origin. Based on the presence of this cycle in multiple satellite datasets, we attribute it to variations in viewing angle during the 16-day orbit repeat cycle of sun-synchronous satellites maintained in Low Earth Orbit (LEO). A 5-point averaging correction procedure is tested on satellite observations from Kilauea volcano, Hawaii, and is found to reduce the impact of higher frequency cycles and reveal the presence of longer-period geophysical signals. In addition to the identification of a signal common to different measurement techniques, an underlying cyclical pattern was found in the OMI SO_2 observations (periods of ~7.9 and 3.2 days) generated by the OMI Row Anomaly (ORA). We conclude that identification of the presence and magnitude of non-geophysical cyclic behaviour, which can suppress natural cycles in time-series data, and implementation of appropriate corrections, is crucial for accurate interpretation of satellite observations. The use of data averaging to suppress non-geophysical cycles imposes limits on the length of natural cycles that can be confidently identified in moderate resolution satellite observations from polar-orbiting spacecraft.

1. Introduction

Satellite remote sensing is an essential tool for the monitoring and assessment of environmental systems. Whether in the elucidation of subsurface processes (Lu, 2007), changes in land use (Lambin & Strahlers, 1994), natural hazard assessment and mitigation (Tralli, Blom, Zlotnicki, Donnellan, & Evans, 2005), or atmospheric conditions (Martin, 2008), satellite measurements are expanding our capability to assess the impacts of both natural and anthropogenic change in near real time and on a global scale. Volcanic systems are dynamic and unpredictable in nature with multiple mechanisms potentially responsible for initiating or sustaining eruptions. Due to this complexity, it is not feasible to quantify all the possible driving forces contributing to eruptions that would be necessary for accurate model construction (Sparks, 2003). Therefore, forecasting of volcanic eruptions tends to focus on past behaviour; i.e., the identification and classification of historic volcanic activity allowing the calculation of recurrence rate which can be incorporated into models (Denlinger & Hoblitt, 1999; Dzierma & Wehrmann, 2010; Odbert, Stewart, & Wadge, 2014; Sparks, 2003; Swanson & Holcomb, 1990; Voight et al., 1999). This method can be effective at volcanic systems characterized by relatively stable activity, where factors such as the chemical composition of the source magma and the conduit dimensions in the subsurface plumbing system show little temporal variability (Jaupart & Allègre, 1991; Papale, Neri, & Macedonio, 1998; Wilson, Sparks, & Walker, 1980). At volcanoes where activity displays repetitive characteristics, time-series analysis can be utilised to identify the duration and offset of the cycles present, with the goal of forecasting periods when resurgent activity should be expected (Odbert et al., 2014). The extended resurgence period typical

* Corresponding author.
E-mail address: vjflower@mtu.edu (V.J.B. Flower).

http://dx.doi.org/10.1016/j.rse.2016.05.022

of volcanic systems requires a data series of significant length and with appropriate temporal resolution to assess the characteristics of volcanic activity. Ground-based measurements have previously been employed in analysis of cyclic behaviour (Nicholson, Mather, Pyle, Odbert, & Christopher, 2013), but can be hindered by the high costs associated with the deployment and maintenance of ground-based equipment, or precluded entirely at very hazardous volcanoes with restricted access. In contrast, moderate resolution satellite-based instruments provide near global daily coverage without the associated cost or risks associated with ground-based monitoring. NASA's polar-orbiting A-Train satellite constellation includes two instruments capable of monitoring volcanic systems on a daily basis: the Ozone Monitoring Instrument (OMI) on Aura and the Moderate Resolution Imaging Spectroradiometer (MODIS) on Aqua. Both OMI and MODIS now offer data records spanning over 10 years, providing near-coincident measurements of volcanic sulphur dioxide (SO_2) emissions and heat fluxes, respectively, with an additional MODIS sensor available on the Terra satellite providing multiple MODIS overpasses per day. To date, there have been few efforts to exploit the synergy of OMI and MODIS in characterizing cyclic volcanic behaviour.

To identify any geophysical variability and trends in satellite observations, interference from instrumental or atmospheric effects must first be identified and removed. Whilst the major interference factors affecting satellite retrievals are generally documented before the release of data (e.g., Krotkov, Carn, Krueger, Bhartia, & Yang, 2006; Wright, Flynn, Garbeil, Harris, & Pilger, 2002), subtler variations can go unidentified in visual inspection of data in the time domain. Through the use of spectral density estimation, patterns can be distinguished in data obtained from satellite instruments (e.g., Murphy, Wright, Oppenheimer, & Souza Filho, 2013; Flower & Carn, 2015); these may be interpreted either as a result of natural processes or as artefacts of the measurement techniques employed. In this paper we discuss the identification of cycles in satellite-based time series data from active volcanoes and their attribution, based on an extensive analysis of OMI and MODIS observations. The near-coincidence of OMI and Aqua/MODIS measurements from the A-Train minimizes any impact of variable volcanic activity or atmospheric conditions on the analysis, and hence analysing the datasets in concert provides unique insight into the origin of cyclic signals. Our conclusions have broad implications for the interpretation of results from time-series analysis of moderate resolution satellite observations of volcanic activity, and are also relevant to any observations of sub-pixel scale phenomena from space.

2. Methodology

2.1. SO_2 emissions

SO_2 is commonly emitted in both effusive and explosive phases of volcanic eruptions and during passive, non-eruptive degassing (Bluth, Schnetzler, Krueger, & Walter, 1993; Carn et al., 2003; Carn, Clarisse, & Prata, 2016; McCormick et al., 2013). Due to its strong absorption bands in the ultraviolet (UV) spectral region (e.g., Bogumil et al., 2003), as well as its relatively low abundance in the atmosphere compared to other volcanic gases such as water vapour and carbon dioxide (CO_2), SO_2 is the main target for remote sensing of volcanic eruptions and degassing (Krotkov et al., 2006; Krueger, 1983). The dynamic and unpredictable nature of volcanic activity requires timely assessment and continuous monitoring of volcanic systems. However, due to safety and logistical concerns, in many locations continuous ground-based monitoring is not feasible, whereas satellite remote sensing provides a safe and effective means of global volcano monitoring (Carn, Krotkov, Yang, & Krueger, 2013). Whilst multiple UV satellite sensors provide tropospheric SO_2 measurements (e.g., the Scanning Imaging Absorption Spectrometer for Atmospheric Chartography [SCIAMACHY]; Lee, Richter, Weber, & Burrows, 2008; OMI; Krotkov et al., 2006; the Global Ozone Monitoring Experiment-2 (GOME-2); Rix et al., 2009; the Ozone Mapping and Profiler Suite [OMPS]; Carn, Yang, Prata, & Krotkov, 2015), OMI currently provides the best spatial resolution (13 × 24 km at nadir) whilst maintaining near-global daily coverage (Krotkov et al., 2006). Operational Level 2 OMI SO_2 data (OMSO2) are publicly available from the NASA Goddard Earth Sciences (GES) Data and Information Services Center (DISC; http://disc.sci.gsfc.nasa.gov/Aura/data-holdings/OMI/omso2_v003.shtml), providing daily, global measurements of SO_2 total column amounts (in Dobson Units (DU); 1 DU = 2.69×10^{16} molecules/cm^2). Operational OMSO2 data are currently processed with a linear fit (LF) algorithm (Yang et al., 2007) using UV radiances measured by OMI in 10 discrete wavelength bands. The typical uncertainty on SO_2 columns retrieved by the LF algorithm is ~20% below 100 DU; above this column amount non-linear absorption effects, which are not accounted for in the algorithm, greatly increase the uncertainty (Yang et al., 2007). However, SO_2 column amounts >100 DU are only present transiently in the core of fresh volcanic eruption clouds and hence are not expected to impact our analysis significantly. The presence of cloud can impact the retrieval of SO_2, with overlying meteorological clouds masking volcanic plumes at lower altitude due to increased scattering of radiation, whilst plumes present above the cloud tops are susceptible to overestimation of SO_2 columns due to multiple scattering effects (Carn et al., 2013).

Accurate retrieval of SO_2 column amounts also requires a-priori knowledge of the injection altitude of the SO_2, which is not available at the LF algorithm runtime and hence must be assumed. Volcanic SO_2 column amounts in the OMSO2 product are calculated for three predefined SO_2 vertical profiles corresponding to the lower troposphere (TRL; SO_2 centre of mass altitude (CMA) of ~3 km), mid-troposphere (TRM; CMA of ~8 km) and the lower stratosphere (STL; CMA of ~17 km) (Yang et al., 2007; Carn et al., 2013). The most appropriate SO_2 vertical profile is selected based on the nature of the volcanic activity under observation. For predominantly passive degassing volcanoes the emissions may be assumed to be confined within approximately 1 km of the summit making the TRL (3 km) SO_2 columns the most appropriate for most active volcanoes (Carn et al., 2013) whilst the TRM and STL SO_2 products are representative of moderate and large eruptions (VEI ≤ 3 and VEI ≥ 4, respectively) (McCormick et al., 2013). Due to the major focus of this work on persistent SO_2 emissions, retrievals were obtained from the TRL (3 km) SO_2 product. This may result in overestimation of SO_2 emissions on days when stronger eruptions injected SO_2 to higher altitudes, but because our analysis focuses on temporal trends in volcanic emissions rather than the absolute values obtained, we believe occasional overestimation should not adversely affect the results.

For this analysis, time-series of SO_2 mass were generated by integrating TRL SO_2 column amounts measured by OMI in a 4° square region centred on each target volcano (Table 1). Data were obtained from individual OMI orbits to prevent issues with multiple retrievals from overlapping orbits at high latitudes. If multiple overpasses intersected a sampling region, data were obtained from the swath with the closest to nadir viewing angle over the volcanic target. Variability in the measured SO_2 mass can result from variations in the volcanic emissions, plume altitude, interference from neighbouring volcanoes or meteorological clouds, but are also modulated by variations in OMI pixel size or GIFOV (ground-projected instantaneous field of view) as the sensor viewing geometry changes during a 16-day satellite orbit repeat cycle (Krotkov et al., 2006). The latter effect is most pronounced for sub-pixel scale SO_2 plumes which are averaged over the OMI GIFOV. An additional interference affecting OMI measurements since 2008 is the OMI Row Anomaly (ORA), which has rendered a variable fraction of the OMI swath unusable due to a blockage in the sensor's field of view (FOV) (see: http://www.knmi.nl/omi/research/product/rowanomaly-background.php). Previous studies using time-series analysis techniques have been limited to periods before the development of the ORA to reduce the impact of this feature on output (Flower & Carn, 2015).

Table 1
Target volcanoes included in this analysis, with dominant style of activity and investigated analysis periods.

Code	Volcano	Location	Dominant activity	Analysis periods
AMB	Ambrym	Vanuatu	Two active vents within a 12 km caldera characterized by a lava lake and strombolian eruptions with near continuous degassing (Bani et al., 2012)	01/2005–12/2008[a] 01/2009–12/2013[a] 05/2006–12/2007 05/2008–12/2013
ANT	Anatahan	Mariana Islands	Periodic explosive eruptions producing moderate plumes occasionally accompanied by pyroclastic flows (Siebert, Simkin, & Kimberly, 2010)	01/2005–09/2005 03/2006–06/2006 01/2007–08/2008
AUG	Augustine	Alaska, USA	Increased activity in May 2005 culminating in an explosive eruption in January 2006 generating ash plumes, pyroclastic flows with ongoing lava dome growth (Global Volcanism Program, 2006a)	12/2005–04/2006
BAG	Bagana	Papua New Guinea	Continuous extrusion of lava with intermittent explosive events generating pyroclastic flows (McCormick, Edmonds, Mather, & Carn, 2012)	01/2005–12/2008[a] 01/2009–12/2013[a] Yearly
BEZ	Bezymianny/Kliuchevskoi	Kamchatka, Russia	Bezymianny displays cyclical dome growth and collapse events occasionally accompanied by lava flows and explosive eruptions; whilst Kliuchevskoi shows frequent summit explosive activity often accompanied by flank lava flows (Siebert et al., 2010)	01/2005–12/2008[a] 01/2009–12/2013[a] 11/2005–12/2005 04/2006–12/2006 05/2007–01/2008 07/2008–09/2008 12/2009–02/2010 05/2010–02/2013
DUK	Dukono	Indonesia	Continuous mild-moderate explosive eruptions generating SO_2 and ash plumes (Global Volcanism Program, 2011a)	01/2005–12/2008[a] 01/2009–12/2013[a] Yearly
ETN	Etna	Italy	Continuous activity characterized by persistent degassing and explosions at the summit with lava flows generated on the flanks of the volcano (Bonaccorso et al., 2011)	01/2005–12/2008[a] 01/2009–12/2013[a] 12/2005–12/2005 07/2006–12/2006 03/2007–04/2008 05/2008–07/2009 04/2010 08/2010–04/2013 09/2013–12/2013
FUG	Fuego	Guatemala	Eruptions dominated by lava flows, and explosions generating pyroclastic flows (Lyons, Waite, Rose, & Chigna, 2010)	01/2005–12/2008[a] 01/2009–12/2013[a] Yearly
KRG	Karangetang	Indonesia	Frequent explosive eruptions and lava dome growth occasionally accompanied by pyroclastic flows (Global Volcanism Program, 2011b)	01/2005–12/2008[a] 01/2009–12/2013[a] 01/2005–08/2005 06/2006–10/2007 11/2008–03/2010 08/2010–12/2010 03/2011–08/2011 05/2012–09/2013
KTH	Karthala	Comoros	Periodic explosive eruptions followed by the formation of transient lava lakes (Global Volcanism Program, 2006b)	01/2005–12/2008[a] 01/2009–12/2013[a] 04/2005 11/2005–12/2005 05/2006–06/2006 01/2007
KMS	Karymsky	Kamchatka, Russia	Periodic explosive eruptions accompanied by lava flows (Siebert et al., 2010)	01/2005–12/2008[a] 01/2009–12/2013[a] Yearly
KLT	Kelut	Indonesia	Lava dome growth with mild-moderate explosive activity (Global Volcanism Program, 2008)	10/2007–04/2008
KIL	Kilauea	Hawaii, USA	Since 2008, persistent summit lava lake generating continuous SO_2 emissions, with lava flows from East Rift Zone vents (Mangan, Cashman, & Swanson, 2015)	01/2005–12/2008[a] 01/2009–12/2013[a] 01/2005–06/2007 07/2007–03/2011 04/2011–07/2011 08/2011–12/2013
LPV	Lopevi	Vanuatu	Vulcanian to sub-plinian eruptions with frequent degassing and occasional lava flows generated following vigorous explosion (Bani et al., 2012)	01/2005–03/2005 10/2005–08/2006 04/2007–05/2007 02/2008
MYN	Mayon	Philippines	Mild-moderate explosive activity generating lava flows (Global Volcanism Program, 2006c, 2007)	08/2005 02/2006 07/2006–10/2006 08/2008 09/2009–01/2010 04/2013
MRP	Merapi	Indonesia	Cyclical lava dome growth and collapse on a time scale of 4–6 years (Pallister et al., 2013)	03/2006–08/2007 10/2010–07/2012
NRZ	Nevado del Ruiz	Colombia	Moderate explosive events in 2012 with ongoing degassing (Global Volcanism Program, 2012a)	02/2012–07/2013
NYG	Nyiragongo	DR Congo	Continuous degassing from persistent lava lake (Tedesco et al., 2007)	01/2005–12/2008[a] 01/2009–12/2013[a] Yearly
PCY	Pacaya	Guatemala	Frequent strombolian activity with intermittent lava flows and occasional moderate explosive eruptions	01/2005–12/2008*

Table 1 (*continued*)

Code	Volcano	Location	Dominant activity	Analysis periods
			(Rodriguez et al., 2004)	01/2009–12/2013*
				01/2005–10/2010
				03/2013–12/2013
PGN	Pagan	Mariana Islands	Mild eruption generating SO_2 and ash emissions (Global Volcanism Program, 2012b)	12/2006
				04/2009
				05/2010–08/2010
				03/2011–08/2011
PDF	Piton de la Fournaise	Réunion	Effusive eruptions periodically occur at a rate of ~3 events/year with a significant caldera collapse occurring in 2007 (Froger et al., 2015)	01/2005–12/2008*
				01/2009–12/2013*
				02/2005
				10/2005–12/2005
				07/2006–03/2007
				09/2008–02/2009
				11/2009–01/2010
				10/2010–12/2010
POP	Popocatepetl	Mexico	Activity is characterized by open vent explosion and passive degassing (Roberge, Delgado-Granados, & Wallace, 2009)	01/2005–12/2008*
				01/2009–12/2013[a]
				Yearly
RBL	Rabaul	Papua New Guinea	Persistent degassing with frequent emissions of ash and periodic mild-severe explosive activity (McCormick et al., 2012)	01/2005–12/2008[a]
				01/2009–12/2013[a]
				01/2005–02/2006
				08/2006–01/2010
				07/2010
				03/2011–08/2011
				01/2013–12/2013
STM	Santa Maria	Guatemala	Persistent lava dome growth at Santiaguito accompanied by minor explosions; periodic larger explosions generate pyroclastic flows and lahars (Global Volcanism Program, 2010)	01/2005–12/2008[a]
				01/2009–12/2013[a]
				Yearly
SMU	Semeru	Indonesia	Persistent strombolian activity with cycles of dome growth and collapse on time scales of 5–7 years generating pyroclastic flows (Kassouk, Thouret, Gupta, Solikhin, & Liew, 2014)	01/2005–12/2008[a]
				01/2009–12/2013[a]
				Yearly
SVL	Shiveluch	Kamchatka, Russia	Cyclical lava dome growth terminating in explosive eruptions generating pyroclastic flows (Siebert et al., 2010)	01/2005–12/2008[a]
				01/2009–12/2013[a]
				Yearly
SHV	Soufriere Hills Volcano	Montserrat	Lava dome growth until 2010 with periodic explosive eruptions and dome collapse events generating pyroclastic flows (Wadge et al., 2014)	01/2005–12/2008[a]
				01/2009–12/2013[a]
				01/2005–02/2010
				03/2010–12/2013
STB	Stromboli	Italy	Persistent mild strombolian explosions and sporadic effusive eruptions (Barberi, Civetta, Rosi, & Scandone, 2009)	01/2005–12/2008[a]
				01/2009–12/2013[a]
				Yearly
TNK	Tinakula	Solomon Islands	Mild-moderate explosive eruptions producing gas and ash plumes (Global Volcanism Program, 2006d)	01/2005–12/2008[a]
				01/2009–12/2013[a]
				02/2006–11/2007
				09/2008–10/2012
TNG	Tungurahua	Ecuador	Explosive eruptions accompanied by ash emissions, pyroclastic flows and lava flows (Steffke, Fee, Garces, & Harris, 2010)	01/2005–12/2008[a]
				01/2009–12/2013[a]
				01/2005–07/2009
				01/2010–07/2010
				11/2010–12/2013
VLR	Villarrica	Chile	Continuous degassing from a lava lake confined in the summit crater with occasional strombolian activity (Dzierma & Wehrmann, 2010)	01/2005–12/2008[a]
				01/2009–12/2013[a]
				01/2005–12/2007
				01/2009–03/2009
				11/2009–04/2012
				07/2013
YSR	Yasur	Vanuatu	Persistent strombolian activity (Bani et al., 2012)	01/2005–12/2008[a]
				01/2009–12/2013[a]
				Yearly

[a] ORA assessment.

2.2. Thermal anomalies

To exploit the synergy offered by NASA's A-Train satellite constellation, we also investigate coincident cyclicity in other observations of volcanic activity. For this we use satellite-based detection of thermal infrared (TIR) anomalies by the MODIS instruments obtained from the MODVOLC thermal alert system (Wright et al., 2002; http: http://modis.higp.hawaii.edu.). Thermal anomalies are caused by increased TIR radiance from volcanic features such as lava lakes, lava flows, and lava domes, and to a lesser extent lava fountains and pyroclastic flows (due to their more transient nature). With the exception of large lava flows, the surface area of these features is typically smaller than a 1×1 km nadir MODIS pixel, and hence the TIR signal is also subject to sub-pixel averaging effects (Steffke & Harris, 2011; Wooster, Rothery, & Kaneko, 1998; Wright et al., 2002; Wright, Flynn, Garbeil, Harris, & Pilger, 2004). MODVOLC incorporates TIR data obtained from both day- and night-time overpasses of two MODIS instruments on-board NASA's Aqua and Terra platforms (Table 2). MODVOLC data consists of spectral radiance ($W\ m^{-2}\ sr^{-1}\ \mu m^{-1}$) obtained from 5 MODIS bands (centred at wavelengths of 3.96, 1.64, 11.03 and 12.02 μm), with two

Table 2
Overview of subdivision characteristics for incorporated data.

Platform	Aura	Aqua			Terra		
Instrument	OMI	MODIS			MODIS		
Identification code	OMI	AMA	AMD	AMN	TMA	TMD	TMN
Measurement characteristics	Daytime	Day and Night-time	Daytime only	Night-time only	Day and Night-time	Daytime only	Night-time only

channels (21 and 22) covering the 3.96 μm band with different dynamic ranges and therefore different saturation temperatures. We use Band 22 radiances unless the saturation temperature (~330 K) is exceeded in which case the Band 21 radiance, with its higher saturation temperature (~500 K) was incorporated (Wright et al., 2002, 2004). Aqua-MODIS is part of NASA's A-Train constellation and hence provides daytime measurements coincident with OMI with an ascending node of 1:30 pm (local time), whilst Terra has a descending node of 10:30 am (local time) (NASA, 2013). Differences between daytime Terra and Aqua MODIS thermal anomaly detection can arise for several reasons, not necessarily of volcanic origin. For example, in tropical regions orographic cloud cover often develops by the early afternoon, and hence a thermal anomaly may be detected in the morning Terra-MODIS overpass, but obscured by clouds in the 1:30 pm Aqua-MODIS measurements. Differences are also expected between the day and night-time MODIS observations from each platform (AMD/AMN, TMD/TMN: Table 2) due to the different alert thresholds implemented for the identification of hot-spots by the MODVOLC algorithm (Wright et al., 2002, 2004). Separate MODVOLC alert thresholds were developed for day and night-time data to prevent the generation of false alerts resulting from diurnal variations in ground surface heating (Wright et al., 2002, 2004). The absence of solar radiation allows the use of a lower threshold in the night-time MODVOLC algorithm, enabling it to distinguish subtler variations in thermal anomalies, which is of particular use in the detection of cooler features such as lava domes or fresh pyroclastic deposits (Wright et al., 2002).

The MODVOLC interface enables the selection of TIR anomalies at a variety of scales from global coverage down to 0.1 × 0.1° latitude and longitude regions centred on known Holocene volcanoes. In this work, thermal alerts for each of our target volcanoes were individually investigated to identify the most appropriate region for data collection. A 0.1 × 0.1° region was used for locations with spatially confined features such as lava lakes or lava domes, minimising the likelihood of incorporating false detections. Alternatively, a 0.5 × 0.5° region provided appropriate coverage where features were more spatially extensive such as lava flows or pyroclastic deposits. For some targets, such as Nyiragongo, activity at a neighbouring volcano (in this case, Nyamulagira) also contributed to the detected TIR anomalies; where this occurred the interfering anomalies associated with activity at the non-target site were removed from the dataset prior to processing (if this resulted in the removal of all anomalies then the value for that day was set to zero). In the light of the possible impacts of variable MODIS viewing geometry and overpass time on the TIR measurements (described above), for our analysis MODVOLC data obtained for each of the target volcanoes (Table 1) were subdivided by satellite and measurement time (Table 2), to reduce the impact of any spurious cyclicity resulting from inconsistent viewing conditions.

2.3. Target volcano selection and time-series analysis

Time-series of daily SO_2 mass and TIR radiance measured over a 9-year period (2005–2013) for 24 volcanoes, with generally persistent activity, were initially analysed to assess whether any common cyclical pattern could be discerned between pre- (2005–2008) and post- (2009–2013) ORA development (Table 1). Following initial assessment, data for each volcano were segregated into individual eruptive phases with continuously active volcanoes segregated for annual analysis and an additional 8 volcanoes, characterized by more sporadic short-lived eruptions, were incorporated. The resulting 32 target volcanoes selected for this analysis (Table 1), display a variability in eruption style, although the main criteria for selection was the availability of sufficient OMI SO_2 and MODVOLC data with minimal extended periods of quiescence. A total of 173 discrete eruptive periods were analysed, in addition to the 48 analyses run on OMI data alone (Table 1). Following data compilation, days with no detected SO_2 or TIR anomaly were assigned a zero value to maintain a continuous time series and a method of analysis developed for the assessment of volcanic cycles at Soufriere Hills Volcano, Montserrat (Flower & Carn, 2015; Nicholson et al., 2013) was employed. This technique incorporates a fast Fourier transform (FFT) multi-taper method (MTM) analysis (Thomson, 1982), facilitating the identification of cycles in datasets where the underlying dynamics of the system are unknown (Percival & Walden, 1993). Output is generated in the form of power spectral density (PSD: signal power as a function of frequency) plots and has been employed in the analysis of a variety of geophysical data (e.g., Flower & Carn, 2015; Lamb et al., 2014; Nicholson et al., 2013; Odbert & Wadge, 2009).

In order to assess the significance of cycles, the dynamics of the data were assessed and determined to display white noise characteristics, with no significant pattern of decreasing power with increasing frequency (Fig. 1); the latter is indicative of red noise and is common in natural systems (Mann & Lees, 1996). White noise confidence limits (95% and 99%) were calculated to facilitate the identification of significant cycles (Duchon & Hale, 2012). Limitations exist with respect to the length of cycles that can be resolved with this technique. Cycles with periods less than the sampling rate (<1 day) cannot be resolved, whilst cycles with periods longer than $n/4$, where n is the length of the initial time series, do not display sufficient recurrences to distinguish them from discrete events within in the data. The final consideration relates to the characteristics of the original data; in this case the orbital geometry (16-day repeat period) of the satellite platforms from which the OMI and MODIS measurements were obtained.

PSD plots were generated for each of the 173 phases of volcanic activity, with OMI and MODIS data subset into seven categories according to the criteria shown in Table 2, for a total of 1211 samples relating to individual eruptive periods with an additional 48 samples from the analysis of OMI data alone. These PSD plots were then used to identify cyclic behaviour common to multiple volcanoes, measurement techniques and observation times to assess the impact of non-volcanic forcing.

3. Results

3.1. OMI row anomaly

A 2.3-day cycle was initially identified as part of a multi-peak PSD feature attributed to the ORA in OMI data compiled for 24 initial sample sites (Table 1). PSD plots for data collected after the development of the ORA display peaks at a frequency of 0.438 cycles day^{-1} (period of 2.3 days) in 16 of the 24 target volcanoes, with only one (Etna) displaying a cycle at this frequency both before and after ORA development. Two further cycles were also identified as common features in the post-ORA PSD plots, at frequencies of 0.124 cycles day^{-1} (8-day period) and 0.312 cycles day^{-1} (3.2 day period), with 19 and 6 sites displaying statistically significant cycles, respectively. Fig. 1 shows PSD plots (2009–2013) for three volcanoes where the influence of the ORA is clearly evident: Pacaya (Guatemala), which exhibits no significant

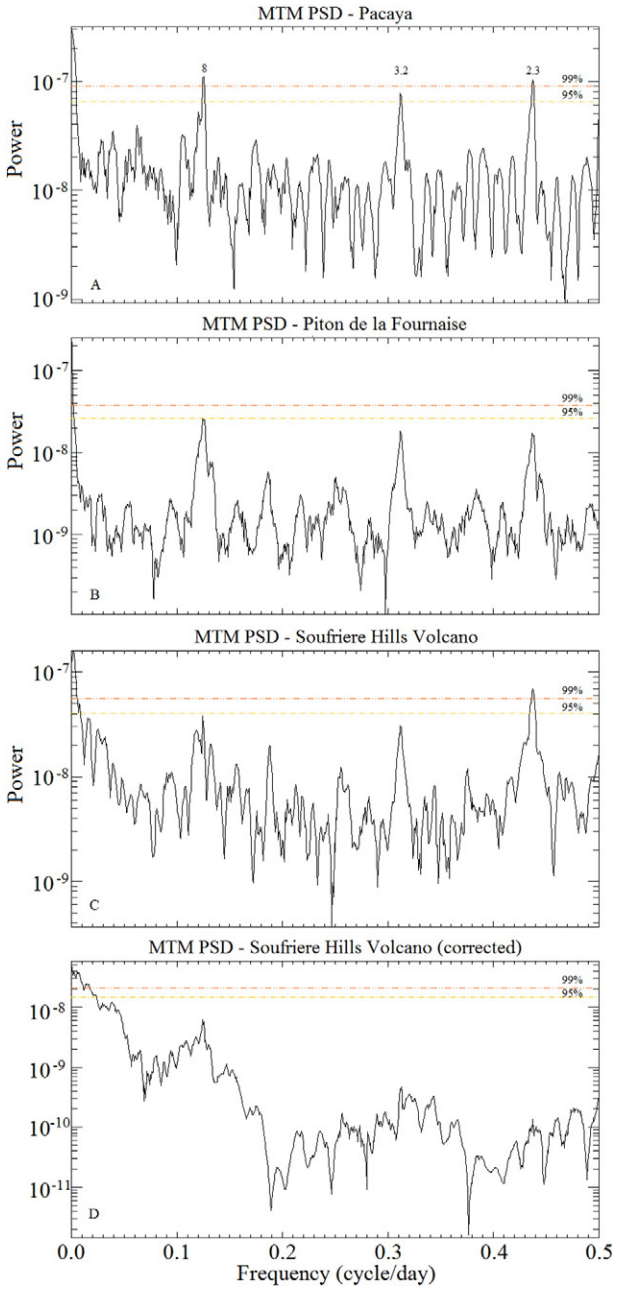

Fig. 1. Characteristic PSD plots for A. Pacaya, B. Piton de la Fournaise and C. Soufriere Hills volcano displaying common ORA cycles (0.124, 0.312, and 0.438), and D. PSD output for Soufriere Hills volcano data treated with 5-point correction.

cycles in the pre-ORA analysis; Piton de la Fournaise (Réunion), which displays only noise prior to the ORA; and Soufriere Hills Volcano (SHV, Montserrat), where significant unrest dominates the pre-ORA analysis (Flower & Carn, 2015), but due to a decrease in activity at SHV roughly coincident with the onset of the ORA, subsequent analysis displays similar characteristics to Pacaya and Piton de la Fournaise. The significant volcanic activity at SHV in 2005–2009 also showed cyclicity with frequencies <0.124 cycles day^{-1} (Flower & Carn, 2015) but despite this the features, which we posit are the result of the ORA, can clearly be identified in all three of these locations (Fig. 1).

In order to accurately assess the presence of cyclical variations in volcanic SO_2 emissions using OMI data affected by the ORA, implementation of an appropriate correction factor would be necessary to prevent the dominance of the ORA feature over any naturally generated cycles. Following the initial identification of this pattern, the OMI SO_2 data were visually assessed to identify the extent and persistence of the ORA. The 16-day repeat cycle of sun-synchronous satellites such as Aura and others in the A-Train constellation results in predictable patterns of ORA interference for a particular location. Initially (in 2008–2011) the location and extent of the ORA in the OMI orbit swath varied, but since July 2011 some stabilisation has occurred (e.g., http://www.knmi.nl/omi/research/product/rowanomaly-background.php) resulting in a reduction in temporal variations. The effect of the ORA through an Aura orbit cycle has been assessed using OMI measurements of SO_2 in the Kilauea (Hawaii) volcanic plume (1st-16th July 2010; Fig. 2). At Kilauea, SO_2 plume dispersion occurs predominantly to the west under typical trade wind conditions and therefore the ORA has greatest impact on measured SO_2 emissions when located west (downwind) of the volcano; and most significant when the ORA is immediately west of and/or over Kilauea, obscuring the highest SO_2 column amounts expected in the young volcanic plume. In general the impact of the ORA at a particular degassing volcano will depend on local variability in wind direction and volcano placement within the OMI swath; volcanoes characterized by relatively invariant wind directions such as Kilauea would be expected to show stronger ORA-induced cyclicity in their measured SO_2 emissions. Table 3 details the relative effect of the ORA on Kilauea SO_2 observations in a single Aura satellite repeat cycle (Fig. 2), highlighting the following patterns:

- Two 3-day segments of the orbit cycle (C–E and J–L) involve severe ORA impacts on alternating days; this is a probable source of the 2.3-day cycle.
- Days with negligible (B, F, I) or mild (K, O) ORA impacts display an average separation equal to the ~3-day cycle.
- The separation between the severely impacted days (i.e., C–J, E–L, N–E) is most likely the source of the 7-day cycle identified in almost 40% of the datasets analysed.

To correct for the data gaps produced by the ORA an appropriate gap-filling methodology is required. Examples of such methodologies used in other studies include: estimation of SO_2 emissions based on the general dynamics of the system (short-term mean calculation or linear interpolation; Nicholson et al., 2013); utilisation of a second instrument with similar measurement capabilities (e.g., OMPS): Telling, Flower, & Carn, 2015), or the use of ground-based remote sensing data to replace missing values. Whilst being of value for estimation purposes, the use of general system dynamics or alternative instruments increases uncertainty as none can provide accurate and comparable coincident measurements with OMI. The deployment of ground-based instrumentation for continuous measurement of SO_2 emissions would provide the appropriate resolution for data replacement, but is not practical for many of the volcanic targets discussed here.

3.2. Viewing angle induced cyclicity

Following the identification of ORA-induced cycles in the OMI SO_2 data, individual periods of volcanic activity were analysed to see if cycles persisted between locations. When combined with the ORA analysis the 2.3-day cycle surpassed the imposed confidence limits in 39 datasets out of a total of 117 showing any significant cyclicity (Table 4). MODVOLC thermal anomalies were analysed for the same periods of unrest at the 32 target volcanoes (Table 1), facilitating comparison with the OMI analyses. TIR radiance detected by the MODVOLC system also exhibited the previously discussed 2.3-day cycle, but by conducting separate analyses of daytime and night-time MODIS data, we find that the persistence of the 2.3-day cycle is dependent on observation time. The analyses summarised in Table 4 indicate that in daytime OMI and MODIS measurements (OMI, AMD, TMD) approximately one-third to half of those analyses identifying any significant cycles detect a significant signal with a period of 2.3 days. In contrast, ~75% of the night-time (AMN,

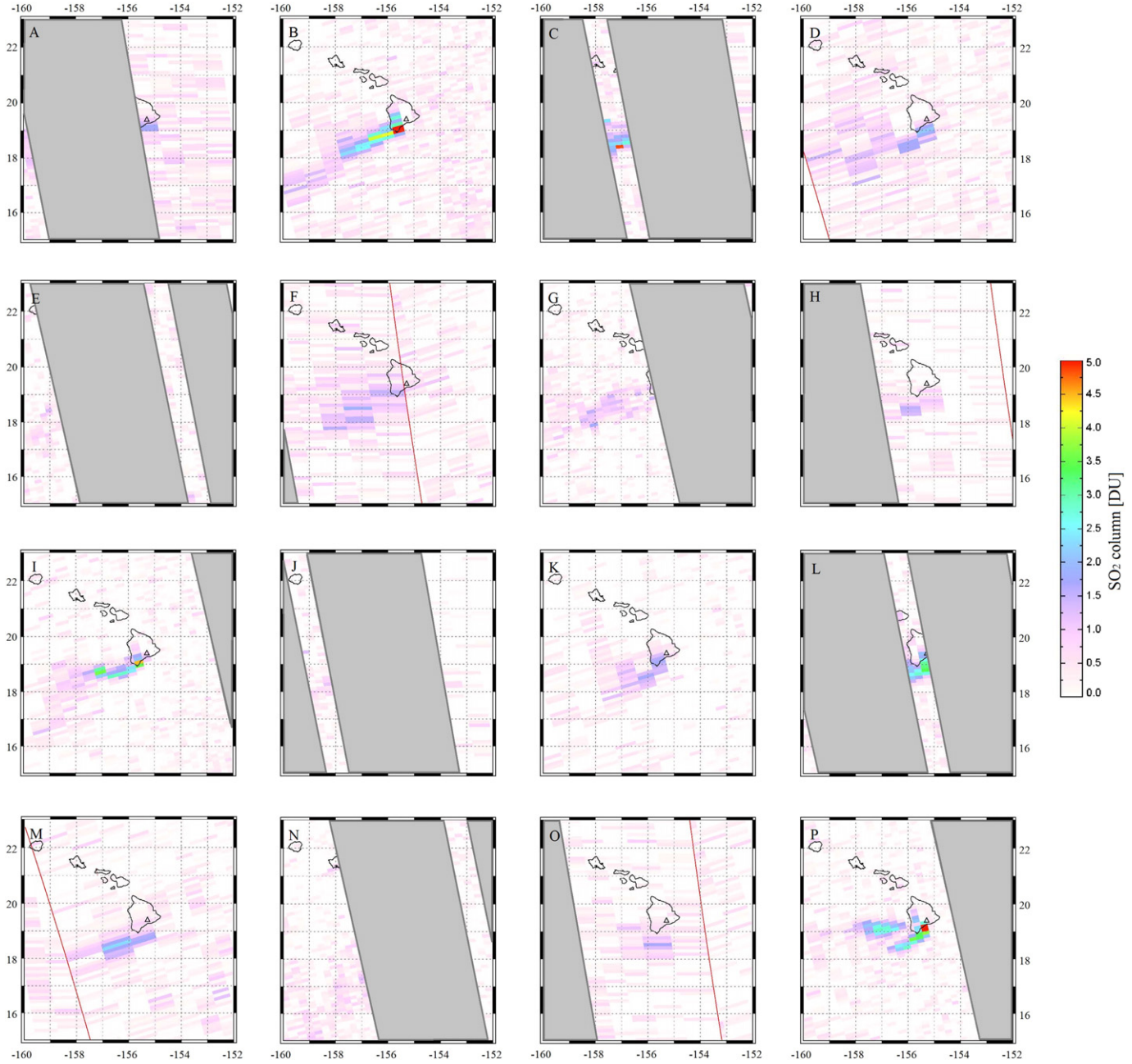

Fig. 2. Regional maps of daily OMI SO_2 data collected over Hawaii, indicating the position and significance of the OMI Row Anomaly generated by variations in viewing angle through a complete progression of Aura's sun-synchronous orbit. Plots A–P correspond to 1st–16th July 2010, respectively. A *triangle* indicates the location of Kilauea volcano.

TMN) and combined (AMA, TMA) MODIS measurements showing any cyclicity display this cycle. The remaining analyses which display cycles were dominated by low frequency features generated by volcanic activity, resulting in suppression of the viewing angle features.

We ascribe this outcome to the increased sensitivity of the nighttime MODVOLC algorithm (Section 2.2), resulting in greater susceptibility to the influence of sensor viewing angle on the detected TIR signal imparted by an increased rate of thermal anomaly detection. A previous study by Murphy et al. (2013) identified cycles of a similar duration in MODIS data whilst investigating MODIS and ASTER synergy at Erta 'Ale (~2 days), Kilauea (2.6 days) and Kliuchevskoi (2.5 days), despite employing a wavelet analysis technique as opposed to the FFT-MTM methodology utilised here. The identified cycles were attributed to the influence of atmospheric phenomena such as cloud cover, resulting in daily variations in TIR radiance associated with otherwise stable sources of TIR radiation (Murphy et al., 2013). Whilst meteorological factors could produce this signal in some of the locations analysed here, its consistency on such a widespread scale suggests that an alternative cause is more likely.

We attribute the persistence of this cycle in OMI and MODIS observations to a common characteristic of the measurements, namely the variation in sensor viewing angle during the 16-day Aura, Aqua and Terra orbit repeat cycles. For example, smaller and/or lower temperature phenomena, or a hot vent, lava lake or lava dome obscured by crater walls (e.g., Wooster et al., 1998), may only be detected by MODIS at nadir (i.e., at peak spatial resolution of 1×1 km), with the increased spatial averaging in the larger off-nadir GIFOV reducing the signal below the threshold of detection, resulting in an otherwise stable thermal feature seeming to wax and wane throughout the satellite orbit cycle. At low latitudes there are also gaps between adjacent MODIS orbital swaths near the equator; these gaps influence some low latitude regions more significantly than others and could result in data gaps on

Table 3
Relative effect of the ORA on OMI SO_2 measurements at Kilauea volcano, Hawaii during one Aura satellite repeat cycle.

Date (July 2010)	Fig. 2 plate	Extent of ORA influence on volcanic SO_2 detection	Overall effect of ORA
1st	A	Plume dispersion further than 2° west obscured	Moderate
2nd	B	Only far extent of large westerly plumes affected	Negligible
3rd	C	Complete obscuration of the volcano and westerly plume dispersion	Severe
4th	D	Plume dispersion further than 4° west obscured	Mild
5th	E	Complete obscuration of the volcano and general dispersion	Severe
6th	F	Only far extent of large westerly plumes affected	Negligible
7th	G	Plume dispersion above volcano and to the east obscured	Moderate
8th	H	Plume dispersion further than 3° west obscured	Moderate
9th	I	Only far extent of rare easterly plumes would be affected	Negligible
10th	J	Any westerly dispersion obscured	Severe
11th	K	Only far extent of large westerly plumes affected	Mild
12th	L	Complete obscuration of the volcano and general dispersion	Severe
13th	M	Plume dispersion further than 3° west obscured	Moderate
14th	N	The volcano, localised and easterly dispersion obscured	Severe
15th	O	Only far extent of large westerly plumes affected	Mild
16th	P	Plume dispersion to the east obscured	Moderate

alternating days, further enhancing the spectral power associated with the ~2.3 day cycle. Similar reasoning can be applied to the OMI SO_2 measurements. Volcanic SO_2 plumes covering areas significantly less than the size of an OMI footprint (13 × 24 km at nadir) would also be subject to variable spatial dilution effects over an Aura orbit cycle, with the measured SO_2 mass approaching or commensurate with background noise levels at extreme viewing angles (larger GIFOVs).

4. Discussion

4.1. Cycle characteristics

The strength of the observed cyclic variations in OMI and MODIS measurements appears to be a function of the latitude of the volcano in addition to the dominant style of volcanic activity. Fig. 3 depicts the persistence of the 2.3-day cycle in OMI and MODIS observations, in addition to the ~3- and ~8-day cycles in OMI measurements, at each of the target volcanoes. Tropical volcanoes (i.e., at absolute latitudes of ≤20°) appear to display greater overall susceptibility to the effects of satellite viewing angle than those at higher latitudes, which is most likely the result of minimal overlap or gaps between orbits (in the case of MODIS) at low latitudes. However, there is a subset of tropical volcanoes that displays little influence of these multi-day cycles (Fig. 3). These volcanoes are characterized by shorter periods of unrest (average durations of 50–275 days; Table 1) relative to those showing stronger cyclicity (average duration of 820 + days; Table 1), and hence the number of observations is likely insufficient for cyclicity to be manifested. Conversely, we note that the group of volcanoes showing the strongest cyclicity includes many of the strongest and most persistent global sources of volcanic SO_2 emissions of the past decade, based on OMI SO_2 measurements since 2004 (Carn et al., 2016).

Villarrica shows the strongest influence of the multi-day cycles of all mid-latitude volcanoes (absolute latitude of 30°–50°), and appears to be an outlier relative to other volcanoes at similar latitudes (Fig. 3), but further analysis reveals that this location shows an ~8-day cycle in all OMI and MODIS analyses. The presence of this cycle in the MODIS data (the ~8-day cycle is a feature of the ORA and does not appear to be characteristic of the MODIS datasets analysed here) implies that it is likely a result of volcanic activity coupled with satellite viewing geometry producing a false positive in the record. Specifically, activity at Villarrica since 2004 has been characterized by a lava lake with a small surface area (2–30 m) residing at variable depths within the summit crater (Witter, Kress, Delmelle, & Stix, 2004; Palma, Calder, Basualto, Blake, & Rothery, 2008; Sawyer et al., 2011), which would be generally obscured from view except during near-nadir MODIS overpasses, thus generating an ~8 day cycle. When the instances of this cycle at Villarrica are removed (Fig. 3; VLR*) the modified analysis is more consistent with that for Stromboli and Etna, and the overall pattern is a decreasing influence of the satellite-viewing-angle-induced, 2.3-day cycle with increasing latitude. The most likely reason for this is the convergence of adjacent sub-satellite orbit tracks at higher latitudes, which effectively reduces viewing angle variations during an orbit repeat cycle (i.e., the average distance of a given target from nadir is reduced). In OMI SO_2 measurements, an additional factor could be the typically lower wind

Table 4
Persistence of common identified cycles in MODIS and OMI observations.

Measurement classification	Total # phases run	Total # runs with cycles detected	Total # of runs with 2.3-day cycle detected
AMA	173	102	78
AMD	173	59	25
AMN	173	103	79
TMA	173	106	76
TMD	173	66	34
TMN	173	103	73
Total MODIS	**1038**	**539**	**365**
OMI	221	117	39
Total	**1259**	**656**	**404**

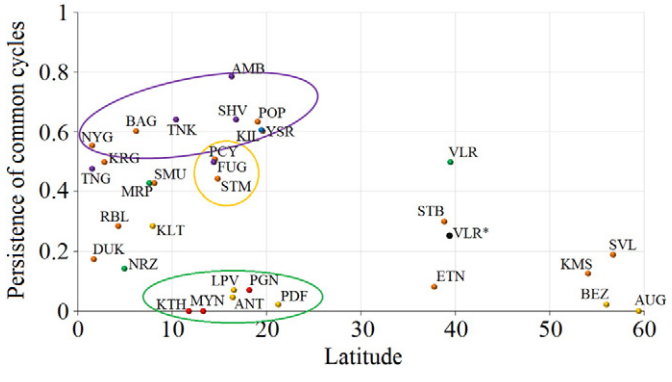

Fig. 3. Persistence of common cyclicity (defined as the fraction of all MTM analyses for each volcano showing a 2.3-, 3- or 8-day cycle) as a function of latitude for all target volcanoes (for corresponding codes see Table 1). Data points are colour coded based on the average number of days within the analysed eruption periods (red < 100 days, orange < 300 days, yellow < 500, green < 750, blue < 1000 and purple 1000 + days). Three regions are outlined, indicating: mid-latitude volcanoes with shorter periods of unrest (50–275 days) which display minimal cyclicity (*green*); the strongest influence of the cycles present in low- to mid-latitude volcanoes with more persistent activity (820 + days; *purple*); and clustering of Guatemalan volcanoes despite variations in time-series length (365 vs 1217 days; *orange*). The black data point for Villarrica (VLR*) represents a corrected value due to the presence of volcanic cyclicity at the same frequency as that generated by sensor viewing geometry.

speeds and lower directional wind shear in the tropics, which limits SO_2 plume dispersion across the OMI GIFOV, i.e., the average spatial extent of volcanic SO_2 plumes may be lower in the tropics.

Some clustering of sites displaying similar activity and geographic location is apparent in Fig. 3; for example, all targets in Guatemala (*orange*) display similar characteristics despite differences in the number of MTM runs conducted (2 vs 9) and average length of time-series (365 vs 1217 days). In OMI SO_2 measurements (unlike MODIS TIR measurements), interference between nearby volcanoes is inevitable as emissions may drift large distances from the source, and common cyclicity in this case may suggest a single dominant SO_2 source in the region affecting all the Guatemalan targets. In a separate study, we have found that comparison of common cyclicity in OMI SO_2 and MODIS TIR observations in regions with multiple active volcanoes can be used to identify the dominant SO_2 source (Flower, 2015). Comparison of the cycles identified in OMI SO_2 data at Fuego, Pacaya and Santa Maria (see Supplementary data) indicates the presence of similar cycles at both Fuego and Santa Maria in 2006 and 2012. Analysis of MODIS data for these years reveals similar cycles at Fuego, indicating that this was the dominant source of volcanic SO_2 emissions in Guatemala in 2006 and 2012. With the identified contaminated cycles removed from the Santa Maria analysis the persistence drops from 0.47 to 0.44, which still maintains the similarities previously identified between the Guatemalan volcanoes (Fig. 3). Whilst the greater number of MODIS samples for each location could bias the analysis towards cyclicity in MODIS data, investigation of the persistence of cycles in both the OMI and MODIS at Santa Maria following the removal of contaminated signals was 0.44.

4.2. Cycle suppression

Here, we discuss possible strategies to mitigate the effects of induced cycles on interpretation of time-series satellite observations, and facilitate the identification of real trends. The strength of moderate resolution, LEO satellite instruments such as OMI and MODIS lies in their ability to provide near-global, daily time series, and hence any correction factor applied to account for cyclical variability would ideally maintain the original temporal resolution (~1 day) of the data. We therefore adopt an averaging rather than a binning methodology to maintain temporal resolution, and through the averaging procedure we reduce the significance of high frequency noise that dominated the earlier analyses. However, this method does result in the suppression of sharp peaks in emissions and therefore would not be appropriate for analysis of short-period pulses of SO_2 associated with explosive eruptions.

Episode 58 of the ongoing eruption of Kilauea, Hawaii (July 2007–March 2011) was used as a test case for correction techniques, as TIR anomalies persisted throughout the MTM analysis of each of the MODIS datasets (Aqua and Terra day- and night-time data). Three methods of data pre-processing were trialled and then analysed with the original MTM methodology;

- Each data point n recalculated as 3-point running average (n_{-1} to n_{+1})
- Each data point n recalculated as 5-point running average (n_{-2} to n_{+2})
- Each data point n recalculated as 7-point running average (n_{-3} to n_{+3})

The averaging of each datum with adjacent values maintains the total number of data points and preserves the general dynamics of the time series, whilst reducing the day-to-day variability produced by the sensor viewing angle. Due to the suppression of all cycles in the Aqua MODIS daytime analysis at frequencies below the peak at 0.438 cycles day^{-1} (Fig. 4a), we conducted detailed analysis to assess the impact of the data averaging on the identification of cycles in this dataset. Unsurprisingly, the 3-point average resulted in the least amount of information loss, but it was unable to suppress the viewing

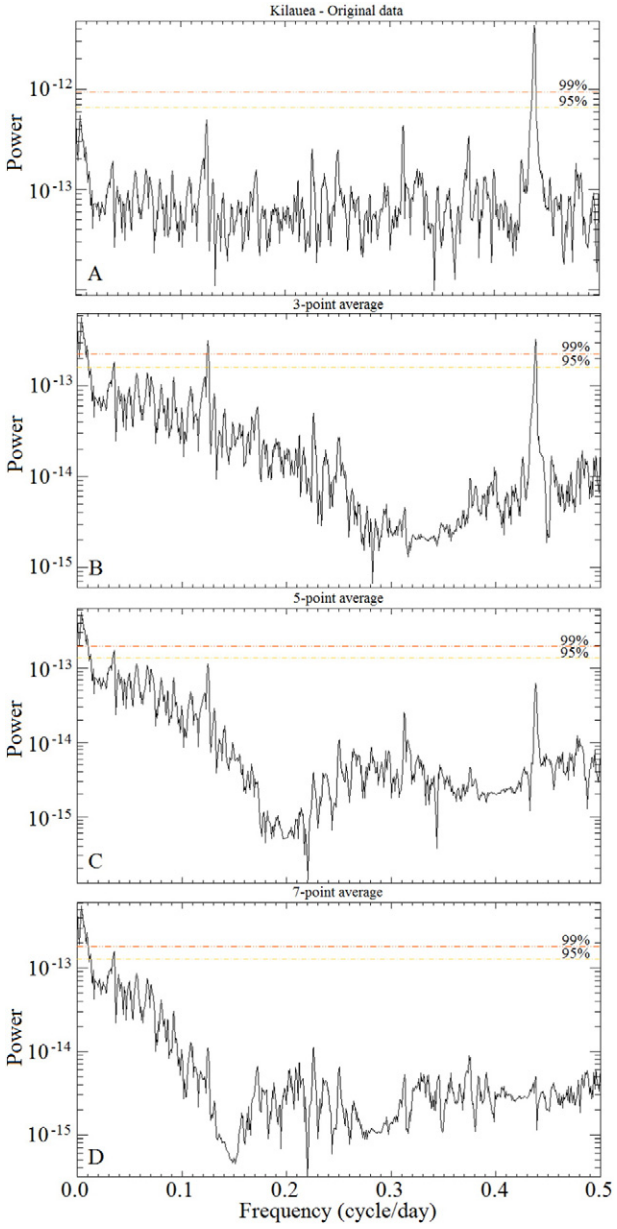

Fig. 4. Effects of data averaging on the PSD output for Aqua daytime MODIS data from Kilauea eruption episode 58 (July 2007–March 2011) with 95% (yellow) and 99% (red) confidence limits. A. No correction applied, B. 3-point correction, C. 5-point correction, D. 7-point correction.

angle effect in all of the analyses, with Aqua MODIS daytime data still displaying a significant peak at 0.438 cycles day^{-1} (Fig. 4b). However, as a result of the suppression of signal power at other frequencies, three peaks exceed designated confidence limits at frequencies of 0.004, 0.036 and 0.125 cycles day^{-1} (periods of ~250, 27 and 8 days; Fig. 4b). The 5-point average (Fig. 4c) suppressed the 2.3-day cycle below the imposed confidence limits and reduced the significance of the 8-day cycle, whilst the longer period cycles appear unaffected in either magnitude or distribution when compared to the 3-point averaging method. Use of a 7-point average resulted in complete suppression of the 2.3-day cycle whilst preserving the ~250- and 27-day cycles (Fig. 4d), but the increased number of samples incorporated into the averaging procedure also resulted in suppression of the 8-day cycle. Based on these results, the 5-point averaging technique was chosen for application to each of the trial datasets for the Kilauea eruption as it provided

an appropriate reduction in the identified artefacts (Fig. 4), with the least impact on the original data. We therefore recommend the inclusion of a 5-point averaging pre-processing step on raw data obtained from LEO satellite instruments to mitigate the impact of the 2.3-day cycle generated by viewing angle variations on time-series analysis. Clearly, application of this technique precludes identification of cycles with equal or shorter period than the averaging window and leads to a drop off of PSD signal towards the frequency corresponding to the number of days averaged (e.g., 5 days = 0.2 cycles day^{-1}).

As with the ORA feature in OMI measurements, the presence of the 2.3-day cycle in MODIS data can suppress natural cycles in the data record due to overwhelming PSD at this frequency. Fig. 5 displays the result of MTM analysis of MODIS data for episode 58 of the ongoing eruption of Kilauea. In general, the signal strength and therefore PSD limits in the Aqua daytime data are considerably lower than those in the Aqua night-time or either Terra datasets. This is due to the 1:30 pm timing of the daytime Aqua satellite overpass, resulting in greater interference from features such as afternoon convective clouds than in the morning Terra overpass. The presence of cloud cover can obscure thermal anomalies, reducing the total power of the samples contained within the Aqua daytime dataset and reducing the overall signal observed within the PSD output. In analyses with no data pre-processing, we find that the 2.3-day cycle dominates each PSD plot, but longer period cycles (~125, ~56 days) do exceed the imposed significance levels to varying degrees in multiple datasets (AMN, TMD, TMN: Fig. 5c, e, g). However, subtler variations are masked by the 2.3-day cycle (AMD: Fig. 5a) as shown by the 5-point averaged data (Fig. 5b, d, f, h). Table 5 details all cycles identified in the original datasets and the 5-point averaging analyses in Fig. 5.

The suppression of the 8-day cycle by the 5-point averaging method suggests the feasibility of its use for correction of ORA-influenced OMI SO_2 data, and therefore a trial was conducted on the post-ORA OMI dataset obtained from SHV (Fig. 1c). Application of this correction suppressed the ORA-induced peaks (0.124, 0.312, 0.438 cycles day^{-1}) and revealed four cycles in the resulting MTM output equating to periods of ~400-, 181-, 74- and 59-days (Fig. 1d). Cycles at periods of 181-, 74- and 54–58-days were identified in the analysis of OMI and/or MODIS data for SHV in 2005–2009 (Flower & Carn, 2015), and were

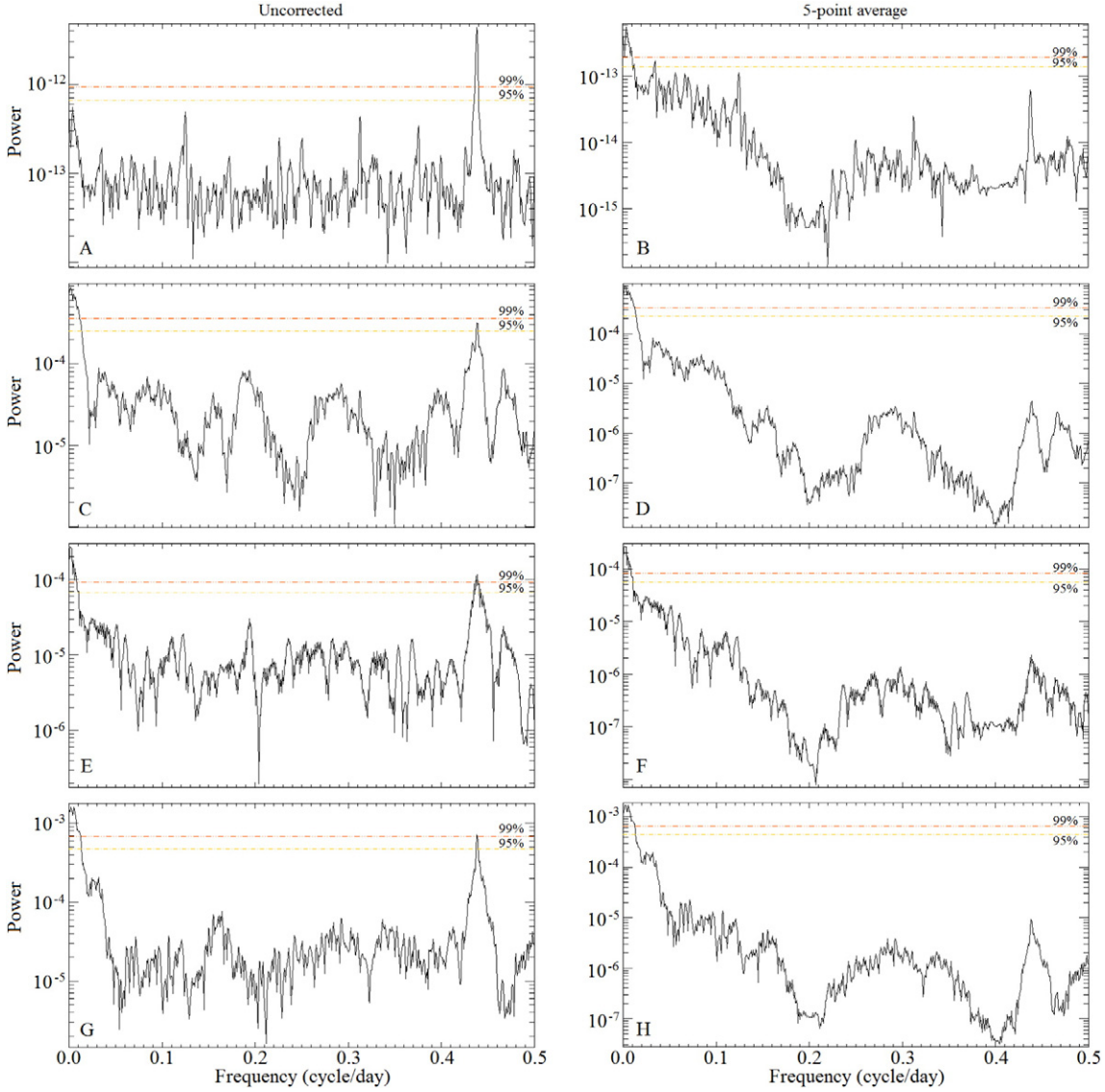

Fig. 5. Comparison of PSD plots computed with uncorrected MODIS data and the selected gap-filling methodology for Kilauea eruption episode 58 (July 2007–March 2011) with 95% (yellow) and 99% (red) confidence limits: A. Aqua daytime (uncorrected), B. Aqua daytime (5-point pre-processing), C. Aqua night-time (uncorrected), D. Aqua night-time (5-point pre-processing), E. Terra daytime (uncorrected), F. Terra daytime (5-point pre-processing), G. Terra night-time uncorrected), H. Terra night-time (5-point pre-processing).

Table 5
Significant cycles (exceeding 95% and 99% confidence limits) identified at Kilauea in the original MODIS analysis and 5-point corrected data series.

	Cycle period (days)			
	No correction applied		5-point correction applied	
Measurement characteristics	99%	95%	99%	95%
Aqua daytime	2.3	–	256, 200, 133, 105	80, 29
Aqua night-time	500, 200, 133, 105, 2.3	78	500, 200, 133, 105	79
Terra daytime	665, 330, 220, 143, 2.3	104	500, 200, 143	95
Terra night-time	435, 200, 109, 90, 2.3	–	500, 200, 133, 100, 80	–

linked to a combination of volcanic and meteorological factors. The identification of these cycles in both pre-ORA and corrected post-ORA data indicates that application of the averaging procedure preserves volcanic or meteorological features in the time-series (provided that any related cycles have periods longer than the averaging window) whilst effectively reducing the influence of instrumental (e.g., viewing angle) effects. The number of data points required for the averaging procedure may vary with geographic location, with targets in equatorial regions more susceptible to the effects of variations in viewing angle (due to the single daily overpass) than those at higher latitudes (where adjacent orbits overlap).

5. Conclusion

Whilst OMI still offers the greatest sensitivity to lower tropospheric volcanic SO_2 plumes of any operational satellite instrument, the development of the ORA can have an impact on time-series analysis of OMI SO_2 data, particularly in equatorial regions, by introducing spurious cyclicity into the observations. Here, we have characterized the impact of the ORA on time-series analysis of OMI SO_2 measurements collected since 2008 at active volcanoes, and have demonstrated how these impacts can be effectively mitigated using a straightforward short term averaging technique. For PSD analysis of OMI SO_2 data affected by the ORA, we recommend application of 5-point averaging to suppress the 8-, 3.2- and 2.3-day cycles associated with this anomaly. This correction permits more accurate assessment of cyclic patterns in volcanic SO_2 emissions in post-ORA data. In some cases, PSD peaks can be assessed and accounted for during interpretation of time-series analysis output, but more subtle cyclic behaviour at volcanoes will be masked by this feature as shown by the post-ORA analysis of data from Soufriere Hills Volcano.

Through power spectral density estimation of 1259 time-series, compiled from OMI SO_2 and MODIS TIR data for 32 persistently active volcanoes, a common signal (0.438 cycles day^{-1}; 2.3 day period) was identified in 61% of datasets displaying any cycles (32% of all targets). This cycle appears most prevalent in night-time MODIS data, with 74% of targets displaying these characteristics. Whilst volcanic cycles could develop at this frequency, based on the persistence of this cycle in multiple locations irrespective of the style of volcanic activity (i.e., degassing, effusive, explosive, dome-forming etc.), we attribute this feature to cyclic variations in sensor viewing angle over the course of LEO satellite repeat cycles. The sensor viewing angle determines the size of the GIFOV, over which the signal associated with sub-pixel sized volcanic plumes or high-temperature features is averaged; hence the impacts described here should be limited to sub-pixel scale phenomena. Furthermore, the presence and strength of such cycles in time-series satellite observations could also be used as evidence for the sub-pixel spatial scale of a target. A 5-point averaging correction procedure was developed and trialled on the MODIS data from Kilauea, and was found to reduce the impact of the 2.3-day cycle, permitting identification of cycles which were otherwise obscured by its presence. The requirement for data averaging imposes limits on the length of natural cycles that can be confidently identified in moderate resolution satellite observations from polar-orbiting spacecraft.

Acknowledgements

We acknowledge NASA for supporting this work through the Aura Science Team project (grant NNX11AF42G to SAC) and an Earth and Space Science Fellowship to VJBF (NNX14AK94H). We thank two reviewers for providing constructive comments that greatly improved the paper.

Appendix A. Supplementary data

Supplementary data to this article can be found online at http://dx.doi.org/10.1016/j.rse.2016.05.022.

References

Bani, P., Oppenheimer, C., Allard, P., Shinohara, H., Tsanev, V., Carn, S., ... Garaebiti, E. (2012). First estimate of volcanic SO 2 budget for Vanuatu island arc. *Journal of Volcanology and Geothermal Research*, *211*, 36–46.

Barberi, F., Civetta, L., Rosi, M., & Scandone, R. (2009). Chronology of the 2007 eruption of Stromboli and the activity of the scientific synthesis group. *Journal of Volcanology and Geothermal Research*, *182*(3), 123–130.

Bluth, G. J. S., Schnetzler, C. C., Krueger, A. J., & Walter, L. S. (1993). The contribution of explosive volcanism to global atmospheric sulphur dioxide concentrations. *Nature*, *366*, 327–329.

Bogumil, K., Orphal, J., Homann, T., Voigt, S., Spietz, P., Fleischmann, O. C., ... Burrows, J. P. (2003). Measurements of molecular absorption spectra with the SCIAMACHY preflight model: Instrument characterization and reference data for atmospheric remote-sensing in the 230–2380 nm region. *Journal of Photochemistry and Photobiology A: Chemistry*, *157*(2), 167–184.

Bonaccorso, A., Bonforte, A., Calvari, S., Del Negro, C., Di Grazia, G., Ganci, G., ... Boschi, E. (2011). The initial phases of the 2008–2009 Mount Etna eruption: A multidisciplinary approach for hazard assessment. *Journal of Geophysical Research: Solid Earth (1978–2012)*, *116*(B3).

Carn, S. A., Krotkov, N. A., Yang, K., & Krueger, A. J. (2013). Measuring global volcanic degassing with the Ozone Monitoring Instrument (OMI). *Geological Society, London, Special Publications*, *380*(1), 229–257. http://dx.doi.org/10.1144/SP380.12.

Carn, S. A., Krueger, A. J., Bluth, G. J. S., Schaefer, S. J., Krotkov, N. A., Watson, I. M., & Datta, S. (2003). Volcanic eruption detection by the Total Ozone Mapping Spectrometer (TOMS) instruments: A 22-year record of sulphur dioxide and ash emissions. *Geological Society, London, Special Publications*, *213*(1), 177–202.

Carn, S. A., Yang, K., Prata, A. J., & Krotkov, N. A. (2015). Extending the long-term record of volcanic SO_2 emissions with the Ozone Mapping and Profiler Suite (OMPS) Nadir Mapper. *Geophysical Research Letters*, *42*, 925–932. http://dx.doi.org/10.1002/2014GL062437.

Carn, S. A., Clarisse, L., & Prata, A. J. (2016). Multi-decadal satellite measurements of global volcanic degassing. *Journal of Volcanology and Geothermal Research*, *311*, 99–134. http://dx.doi.org/10.1016/j.jvolgeores.2016.01.002.

Denlinger, R. P., & Hoblitt, R. P. (1999). Cyclic eruptive behavior of silicic volcanoes. *Geology*, *27*(5), 459–462. http://dx.doi.org/10.1130/0091-7613(1999)027<0459:CEBOSV>2.3.CO;2.

Duchon, C., & Hale, R. (2012). *Time Series Analysis in Meteorology and Climatology: An Introduction*. Advancing Weather and Climate Science: Wiley.

Dzierma, Y., & Wehrmann, H. (2010). Eruption time series statistically examined: Probabilities of future eruptions at Villarrica and Llaima Volcanoes, Southern Volcanic Zone, Chile. *Journal of Volcanology and Geothermal Research*, *193*(1), 82–92.

Flower, V. J. B., & Carn, S. A. (2015). Characterising volcanic cycles at the Soufriere Hills Volcano, Montserrat: Time series analysis of multi-parameter satellite data sets. *Journal of Volcanology and Geothermal Research*, *304*, 82–93. http://dx.doi.org/10.1016/j.jvolgeores.2015.07.035.

Flower, Verity J. B. (2015). Synergistic time-series analysis of satellite data: Applications to volcano monitoring (doctoral dissertation), Michigan Technological University. http://digitalcommons.mtu.edu/etdr/16.

Froger, J. L., Famin, V., Cayol, V., Augier, A., Michon, L., & Lénat, J. F. (2015). Time-dependent displacements during and after the April 2007 eruption of Piton de la Fournaise, revealed by interferometric data. *Journal of Volcanology and Geothermal Research*, *296*, 55–68.

Global Volcanism Program (2006a). Report on Augustine (United States). In R. Wunderman (Ed.), *Bulletin of the Global Volcanism Network, 31:1. Smithsonian Institution.* http://dx.doi.org/10.5479/si.GVP.BGVN200601-313010.
Global Volcanism Program (2006b). Report on Karthala (Comoros). In R. Wunderman (Ed.), *Bulletin of the Global Volcanism Network, 31:1. Smithsonian Institution.* http://dx.doi.org/10.5479/si.GVP.BGVN200601-233010.
Global Volcanism Program (2006c). Report on Mayon (Philippines). In R. Wunderman (Ed.), *Bulletin of the Global Volcanism Network, 31:7. Smithsonian Institution.* http://dx.doi.org/10.5479/si.GVP.BGVN200607-273030.
Global Volcanism Program (2006d). Report on Tinakula (Solomon Islands). In R. Wunderman (Ed.), *Bulletin of the global volcanism network, 31:3 Smithsonian Institution.* http://dx.doi.org/10.5479/si.GVP.BGVN200603-256010.
Global Volcanism Program (2007). Report on Mayon (Philippines). In E. Venzke (Ed.), *Bulletin of the global volcanism network, 32:5. Smithsonian Institution.* http://dx.doi.org/10.5479/si.GVP.BGVN200705-273030.
Global Volcanism Program (2008). Report on Kelut (Indonesia). In R. Wunderman (Ed.), *Bulletin of the Global Volcanism Network, 33:3. Smithsonian Institution.* http://dx.doi.org/10.5479/si.GVP.BGVN200803-263280.
Global Volcanism Program (2010). Report on Santa Maria (Guatemala). In R. Wunderman (Ed.), *Bulletin of the Global Volcanism Network, 35:3. Smithsonian Institution.* http://dx.doi.org/10.5479/si.GVP.BGVN201003-342030.
Global Volcanism Program (2011a). Report on Dukono (Indonesia). In R. Wunderman (Ed.), *Bulletin of the Global Volcanism Network, 36:8. Smithsonian Institution.* http://dx.doi.org/10.5479/si.GVP.BGVN201108-268010.
Global Volcanism Program (2011b). Report on Karangetang (Indonesia). In R. Wunderman (Ed.), *Bulletin of the Global Volcanism Network, 36:1. Smithsonian Institution.* http://dx.doi.org/10.5479/si.GVP.BGVN201102-267020.
Global Volcanism Program (2012a). Report on Nevado del Ruiz (Colombia). In R. Wunderman (Ed.), *Bulletin of the Global Volcanism Network, 37:8. Smithsonian Institution.* http://dx.doi.org/10.5479/si.GVP.BGVN201208-351020.
Global Volcanism Program (2012b). Report on Pagan (United States). In R. Wunderman (Ed.), *Bulletin of the Global Volcanism Network, 37:12. Smithsonian Institution.* http://dx.doi.org/10.5479/si.GVP.BGVN201212-284170.
Jaupart, C., & Allègre, C. J. (1991). Gas content, eruption rate and instabilities of eruption regime in silicic volcanoes. *Earth and Planetary Science Letters*, *102*(3), 413–429.
Kassouk, Z., Thouret, J. C., Gupta, A., Solikhin, A., & Liew, S. C. (2014). Object-oriented classification of a high-spatial resolution SPOT5 image for mapping geology and landforms of active volcanoes: Semeru case study, Indonesia. *Geomorphology*, *221*, 18–33.
Krotkov, N. A., Carn, S. A., Krueger, A. J., Bhartia, P. K., & Yang, K. (2006). Band residual difference algorithm for retrieval of SO 2 from the Aura Ozone Monitoring Instrument (OMI). *Geoscience and Remote Sensing, IEEE Transactions on*, *44*(5), 1259–1266.
Krueger, A. J. (1983). Sighting of El Chichon sulfur dioxide clouds with the Nimbus 7 total ozone mapping spectrometer. *Science*, *220*(4604), 1377–1379.
Lamb, O. D., Varley, N. R., Mather, T. A., Pyle, D. M., Smith, P. J., & Liu, E. J. (2014). Multiple timescales of cyclical behaviour observed at two dome-forming eruptions. *Journal of Volcanology and Geothermal Research*, *284*, 106–121.
Lambin, E. F., & Strahlers, A. H. (1994). Change-vector analysis in multitemporal space: A tool to detect and categorize land-cover change processes using high temporal-resolution satellite data. *Remote Sensing of Environment*, *48*(2), 231–244.
Lee, C., Richter, A., Weber, M., & Burrows, J. P. (2008). SO_2 retrieval from SCIAMACHY using the Weighting Function DOAS (WFDOAS) technique: Comparison with Standard DOAS retrieval. *Atmospheric Chemistry and Physics*, *8*(20), 6137–6145.
Lu, Z. (2007). InSAR imaging of volcanic deformation over cloud-prone areas–Aleutian Islands. *Photogrammetric Engineering & Remote Sensing*, *73*(3), 245–257.
Lyons, J. J., Waite, G. P., Rose, W. I., & Chigna, G. (2010). Patterns in open vent, strombolian behavior at Fuego volcano, Guatemala, 2005–2007. *Bulletin of Volcanology*, *72*(1), 1–15.
Mangan, M. T., Cashman, K. V., & Swanson, D. A. (2015). The dynamics of Hawaiian-style eruptions: A century of study. *Characteristics of Hawaiian Volcanoes*, *323*.
Mann, M. E., & Lees, J. M. (1996). Robust estimation of background noise and signal detection in climatic time series. *Climatic Change*, *33*(3), 409–445.
Martin, R. V. (2008). Satellite remote sensing of surface air quality. *Atmospheric Environment*, *42*(34), 7823–7843.
McCormick, B. T., Edmonds, M., Mather, T. A., Campion, R., Hayer, C. S., Thomas, H. E., & Carn, S. A. (2013). Volcano monitoring applications of the Ozone Monitoring Instrument. *Geological Society, London, Special Publications*, *380*(1), 259–291.
McCormick, B. T., Edmonds, M., Mather, T. A., & Carn, S. A. (2012). First synoptic analysis of volcanic degassing in Papua New Guinea. *Geochemistry, Geophysics, Geosystems*, *13*(3).
Murphy, S. W., Wright, R., Oppenheimer, C., & Souza Filho, C. R. (2013). MODIS and ASTER synergy for characterizing thermal volcanic activity. *Remote Sensing of Environment*, *131*, 195–205.
Nicholson, E. J., Mather, T. A., Pyle, D. M., Odbert, H. M., & Christopher, T. (2013). Cyclical patterns in volcanic degassing revealed by SO_2 flux timeseries analysis: An application to Soufrière Hills Volcano, Montserrat. *Earth and Planetary Science Letters*, *375*, 209–221.
NASA (2013). MODIS http://modis.gsfc.nasa.gov
Odbert, H. M., & Wadge, G. (2009). Time series analysis of lava flux. *Journal of Volcanology and Geothermal Research*, *188*(4), 305–314.
Odbert, H. M., Stewart, R. C., & Wadge, G. (2014). Cyclic phenomena at the Soufrière Hills volcano, Montserrat. *Geological Society, London, Memoirs*, *39*(1), 41–60.
Pallister, J. S., Schneider, D. J., Griswold, J. P., Keeler, R. H., Burton, W. C., Noyles, C., ... Ratdomopurbo, A. (2013). Merapi 2010 eruption—Chronology and extrusion rates monitored with satellite radar and used in eruption forecasting. *Journal of Volcanology and Geothermal Research*, *261*, 144–152.
Palma, J. L., Calder, E. S., Basualto, D., Blake, S., & Rothery, D. A. (2008). Correlations between SO_2 flux, seismicity, and outgassing activity at the open vent of Villarrica volcano, Chile. *Journal of Geophysical Research*, *113*, B10201. http://dx.doi.org/10.1029/2008JB005577.
Papale, P., Neri, A., & Macedonio, G. (1998). The role of magma composition and water content in explosive eruptions: 1. Conduit ascent dynamics. *Journal of Volcanology and Geothermal Research*, *87*(1), 75–93.
Percival, D. B., & Walden, A. T. (1993). *Spectral analysis for physical applications.* Cambridge University Press.
Rix, M., Valks, P., Hao, N., Van Geffen, J., Clerbaux, C., Clarisse, L., ... Emmadi, S. (2009). Satellite monitoring of volcanic sulfur dioxide emissions for early warning of volcanic hazards. *Selected Topics in Applied Earth Observations and Remote Sensing, IEEE Journal of*, *2*(3), 196–206.
Roberge, J., Delgado-Granados, H., & Wallace, P. J. (2009). Mafic magma recharge supplies high CO2 and SO2 gas fluxes from Popocatépetl volcano, Mexico. *Geology*, *37*(2), 107–110.
Rodríguez, L. A., Watson, I. M., Rose, W. I., Branan, Y. K., Bluth, G. J., Chigna, G., ... Fischer, T. P. (2004). SO_2 emissions to the atmosphere from active volcanoes in Guatemala and El Salvador, 1999–2002. *Journal of Volcanology and Geothermal Research*, *138*(3), 325–344.
Sawyer, G. M., Salerno, G. G., Le Blond, J. S., Martin, R. S., Spampinato, L., Roberts, T. J., ... Oppenheimer, C. (2011). Gas and aerosol emissions from Villarrica volcano, Chile. *Journal of Volcanology and Geothermal Research*, *203*, 62–75.
Siebert, L., Simkin, T., & Kimberly, P. (2010). *Volcanoes of the world.* Univ of California Press.
Sparks, R. S. J. (2003). Forecasting volcanic eruptions. *Earth and Planetary Science Letters*, *210*(1), 1–15.
Steffke, A. M., Fee, D., Garces, M., & Harris, A. (2010). Eruption chronologies, plume heights and eruption styles at Tungurahua Volcano: Integrating remote sensing techniques and infrasound. *Journal of Volcanology and Geothermal Research*, *193*(3), 143–160.
Steffke, A. M., & Harris, A. J. (2011). A review of algorithms for detecting volcanic hot spots in satellite infrared data. *Bulletin of Volcanology*, *73*(9), 1109–1137.
Swanson, D. A., & Holcomb, R. T. (1990). *Regularities in growth of the Mount St. Helens dacite dome, 1980–1986. In Lava flows and domes (pp. 3–24)*Berlin Heidelberg: Springer.
Tedesco, D., Vaselli, O., Papale, P., Carn, S. A., Voltaggio, M., Sawyer, G. M., ... Tassi, F. (2007). January 2002 volcano-tectonic eruption of Nyiragongo volcano, Democratic Republic of Congo. *Journal of Geophysical Research: Solid Earth (1978–2012)*, *112*(B9).
Telling, J. W., Flower, V. J. B., & Carn, S. A. (2015). *A multi-sensor satellite assessment of SO2 emissions from the 2012–13 eruption of Tolbachik volcano.* Journal of Volcanology and Geothermal Research: Kamchatka (in review).
Thomson, D. J. (1982). Spectrum estimation and harmonic analysis. *Proceedings of the IEEE*, *70*(9), 1055–1096.
Tralli, D. M., Blom, R. G., Zlotnicki, V., Donnellan, A., & Evans, D. L. (2005). Satellite remote sensing of earthquake, volcano, flood, landslide and coastal inundation hazards. *ISPRS Journal of Photogrammetry and Remote Sensing*, *59*(4), 185–198.
Voight, B., Sparks, R. S. J., Miller, A. D., Stewart, R. C., Hoblitt, R. P., Clarke, A., ... Young, S. R. (1999). Magma flow instability and cyclic activity at Soufriere Hills Volcano, Montserrat, British West Indies. *Science*, *283*(5405), 1138–1142.
Wadge, G., Voight, B., Sparks, R. S. J., Cole, P. D., Loughlin, S. C., & Robertson, R. E. A. (2014). An overview of the eruption of Soufriere Hills Volcano, Montserrat from 2000 to 2010. *Geological Society, London, Memoirs*, *39*(1), 1–40.
Wilson, L., Sparks, R. S. J., & Walker, G. P. (1980). Explosive volcanic eruptions—IV. The control of magma properties and conduit geometry on eruption column behaviour. *Geophysical Journal International*, *63*(1), 117–148.
Witter, J. B., Kress, V. C., Delmelle, P., & Stix, J. (2004). Volatile degassing, petrology, and magma dynamics of the Villarrica Lava Lake, Southern Chile. *Journal of Volcanology and Geothermal Research*, *134*(4), 303–337.
Wooster, M. J., Rothery, D. A., & Kaneko, T. (1998). Geometric considerations for the remote monitoring of volcanoes: Studies of lava domes using ATSR and the implications for MODIS. *International Journal of Remote Sensing*, *19*, 2585–2591.
Wright, R., Flynn, L., Garbeil, H., Harris, A., & Pilger, E. (2002). Automated volcanic eruption detection using MODIS. *Remote Sensing of Environment*, *82*(1), 135–155.
Wright, R., Flynn, L. P., Garbeil, H., Harris, A. J., & Pilger, E. (2004). MODVOLC: Near-real-time thermal monitoring of global volcanism. *Journal of Volcanology and Geothermal Research*, *135*(1), 29–49.
Yang, K., Krotkov, N. A., Krueger, A. J., Carn, S. A., Bhartia, P. K., & Levelt, P. F. (2007). Retrieval of large volcanic SO_2 columns from the Aura Ozone Monitoring Instrument: Comparison and limitations. *Journal of Geophysical Research: Atmospheres (1984–2012)*, *112*(D24).